Journal of Visualization, Vol. 10, No. 1 (2007)47-55

Visualization of the Inflow Ahead of a Rotating Propeller attached to a Container Ship Model

Paik, B. G.*[1], Kim, G. D.*[1], Lee, J. Y.*[2] and Lee, S. J.*[2]

*1 Marine Transportation and Safety Dept., Maritime and Ocean Engineering Research Institute, KORDI, Jang-dong 171, Yuseong-gu, Daejeon, 305-343, Korea. E-mail: ppaik@moeri.re.kr
*2 Department of Mechanical Engineering, Pohang University of Science and Technology, San 31, Hyoja-dong, Pohang, 790-784, Korea.

Received 24 April 2006
Revised 1 August 2006

Abstract : The inflow ahead of a rotating propeller attached to a container ship model was visualized using a two-frame particle image velocimetry (PIV) technique. For illuminating the inflow region, a transparent window was installed at the stern of the ship model. Ensemble-averaged mean velocity fields were measured at four different blade phases under the design loading condition. The characteristics of the inflow in the upper plane above the propeller axis are quite different from those below the propeller axis. In the far upstream region above the propeller axis, most of the inflow comes from the hull wake and the axial velocity is very small. As the inflow moves toward the propeller plane, its axial velocity component increases rapidly. In addition, the variation of the inflow characteristics with respect to phase angle becomes apparent. The thick hull boundary layer and out-of-plane motion resulting from the propeller rotation produce a large turbulent kinetic energy around the tip of the propeller blade in the upper inflow region. The axial velocity distribution of the propeller inflow is asymmetric with respect to the vertical center axis, exhibiting different axial velocities on the port and starboard sides.

Keywords : Two-frame PIV, Propeller inflow, Phase-averaging, Tip vortex, Total velocity.

1. Introduction

The wake formed behind a ship hull greatly influences the performance of the marine propeller driving the vessel; hence accurate analysis of the propeller and hull wake interaction is essential in predicting propeller performance such as propulsion, hydro-acoustic noise and cavitation. The size of the cavity produced by the propeller, as well as pressure fluctuations induced by propeller rotation, is closely related to the characteristics of the propeller inflow. In addition, the propeller inflow is also an important variable because it is used as input data for propeller design and analysis. Although the rudder behind a rotating propeller will affect the hull wake a little in front of a propeller plane, the consideration of the rudder is not included in the present study to investigate the flow structure between propeller and hull.

Numerical predictions of propeller inflows have several limitations, including the use of simplified modeling of propellers, an insufficient description of unsteady interactions, and the assumption of no free surface. Therefore, accurate experimental data on propeller inflow is essential to validate the accuracy and usefulness of numerical models.

As far as we know, the total velocity indicating the velocity of propeller inflow has been measured using an LDV (laser Doppler velocimetry). Lauden (1981) and Lee et al. (1991) measured the inflow velocity of a rotating propeller with an LDV. However, the total velocity data measured at discrete locations were too complicated and the spatial resolution in the measured velocity

distribution was insufficient. Kuiper et al. (2002) also investigated the propeller inflow for full-scale and scale-down models. However, the spatial resolution of measured velocity distribution is not so high. Actually, it is very difficult and needs so much time to measure the inflow region with an LDV since the inflow region is located between a rotating propeller and a ship hull.

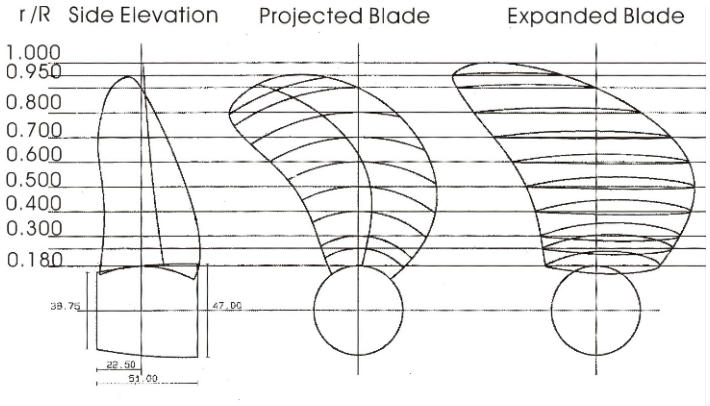

Specification of Kp505 propeller model			
DIAMETER(MM)	: 54.0	SCALE RATIO	: 146.3
(P/D) mean	: 0.950	PROP. TYPE	: FPP
Ae/Ao	: 0.800	SECTION	: NACA66
HUB RATIO	: 0.180	NO. OF BLADES: 5	

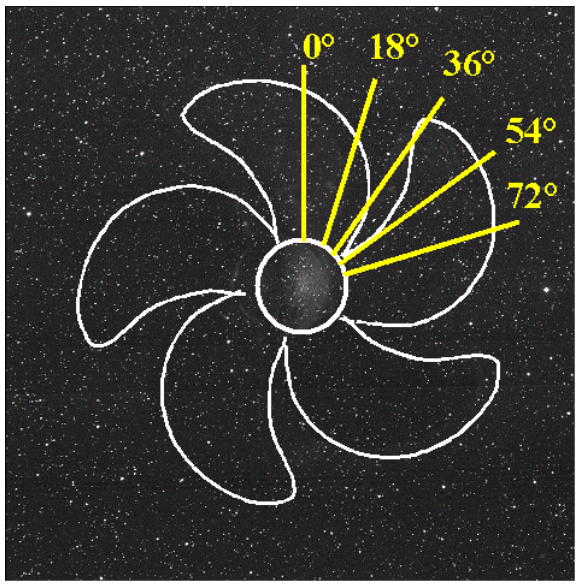

(a) Propeller geometry (b) Phase angels

Fig. 1. Propeller geometry and phase angles of propeller model.

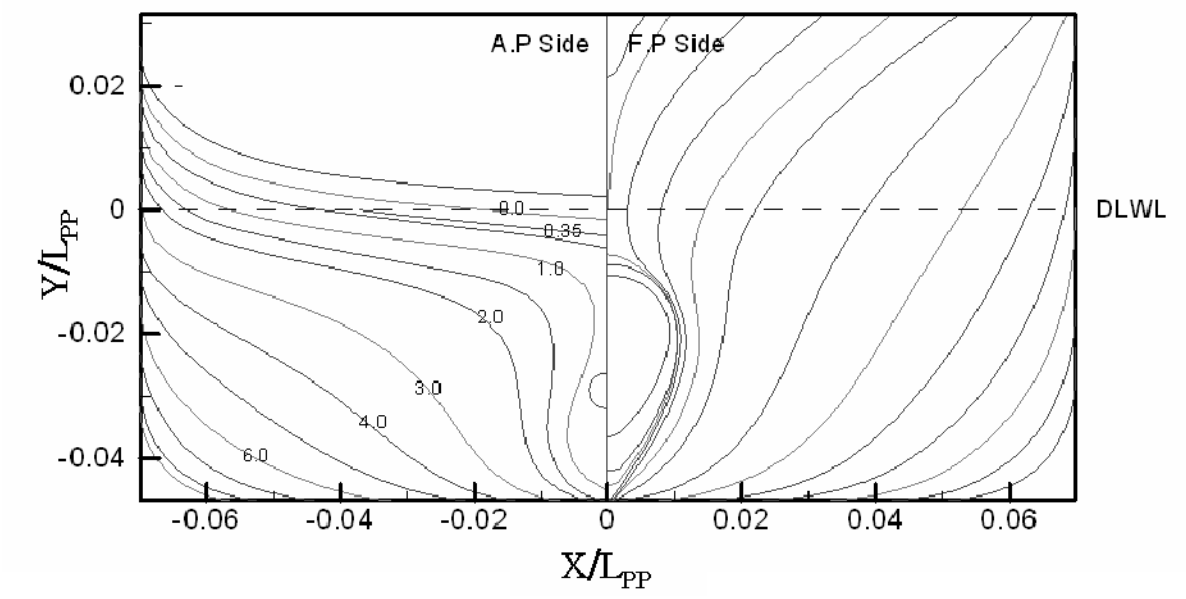

Fig. 2. Body plan of ship model.

Particle image velocimetry (PIV) has been employed recently to measure the velocity fields of the flow behind a rotating propeller. Cotroni et al. (2000) and Lee et al. (2004a) have used PIV and PTV (particle tracking velocimetry), respectively, to investigate the near-wake of an isolated marine propeller in longitudinal planes. Calcagno et al. (2002) and Lee et al. (2004b) investigated the complicated 3-D flow behind a marine propeller in the transverse and longitudinal planes using a stereoscopic PIV (SPIV) technique. Di Felice et al. (2004) measured the propeller wake with PIV technique and they useful information on the influence of propeller loading.

The main objectives of the present study were to visualize the inflow ahead of a rotating propeller attached to KRISO 3600TEU container ship (KCS) model using a phase-averaged PIV technique and to investigate its flow characteristics. In this work, the spatial distributions of the mean flow structure and turbulence statistics of the propeller inflow were elucidated by measuring 400 instantaneous velocity fields at each of four different phases of the propeller blade.

2. Experimental Apparatus and Method

The PIV system used to visualize the propeller inflow is composed of a dual-head Nd:YAG laser, a CCD camera, a time delay generator, and a frame grabber. The CCD camera has a spatial resolution of 2048 × 2048 pixels and can capture pairs of particle images separated by a short time interval with the frame-straddling method. From the captured particle images, velocity fields were extracted using the cross-correlation PIV algorithm. The interrogation windows were 48 × 48 pixels in size and 50% overlapped. The energy of the Nd:YAG laser was 120 mJ per pulse and the time interval between consecutive pulses was fixed at 300 μs. Silver-coated hollow glass beads of 10 μm in mean diameter were seeded as tracer particles.

The experimental model was installed in a circulating water channel. The test section size of channel was $4.5^{L} \times 1.0^{W} \times 1.0^{H}$ m^3. The propeller geometry (KP505) for the KCS and the body plan are described in Figs. 1 and 2. The scaled-down model of KP505 propeller has 5 blades of diameter 54 mm. The free stream velocity (W_0) was fixed at 0.6 m/s. The revolution speed of the propeller for the design condition is 15.43 rps (revolutions per second). The Reynolds number based on the length between the perpendiculars of the ship model is about 9×10^5.and the Reynolds number based on 0.7R(R = radius of propeller) blade chord length is about 3×10^4.

A transparent acryl window was installed at the stern of the ship model through which the inflow region between the propeller and the ship hull was illuminated with a laser sheet. The Nd:YAG laser beam was split into two by a beam splitter, with one beam illuminating the inflow region from above the ship stern and the other illuminating the inflow region from the bottom of the water channel. As a result, the entire inflow region ahead of the propeller was illuminated with a thin laser light sheet of about 2 mm in thickness. The physical size of the field of view was 9.4 × 9.4 cm^2.

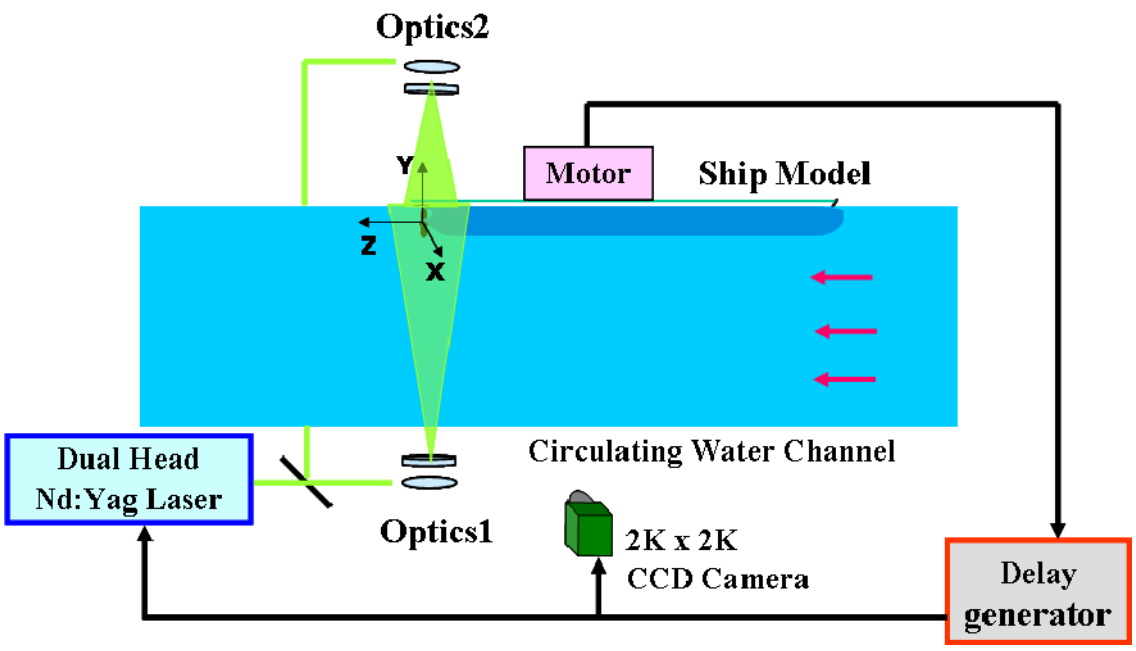

Fig. 3. The schematic diagram of experimental set-up.

Figure 3 shows a schematic diagram of the experimental set-up and the coordinate system used in this study. The CCD camera used to capture particle images was installed outside the water channel. The Z-axis lies along the propeller shaft, pointing toward the stern of the ship; the X-axis is set horizontally toward the starboard, and the Y-axis points upward. The origin is positioned at the center of the propeller boss and all distances are normalized by the propeller diameter D.

The total measurement error is the sum of bias errors and random or precision errors. The error encountered in the determination of displacement vector for an interrogation window is related to the bias error which contributes a certain degree of error, and some degree of a random error. The bias error may be originated from the sub elements of PIV system, such as laser, delay generator and

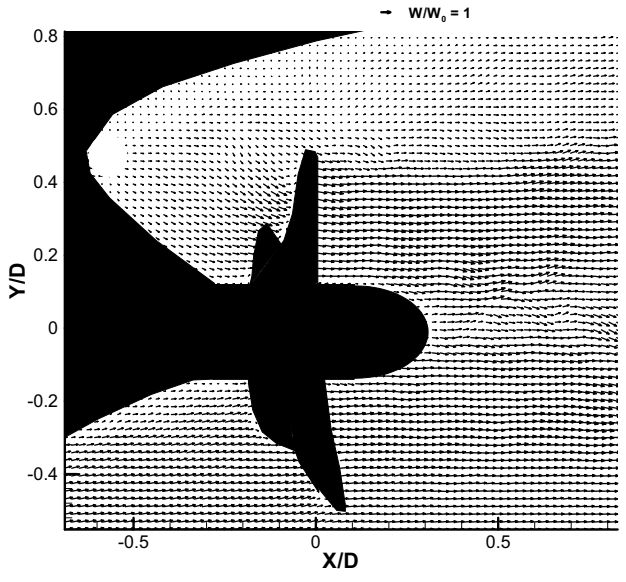

Fig. 4. Typical instantaneous velocity field at the phase angle ϕ = 0°.

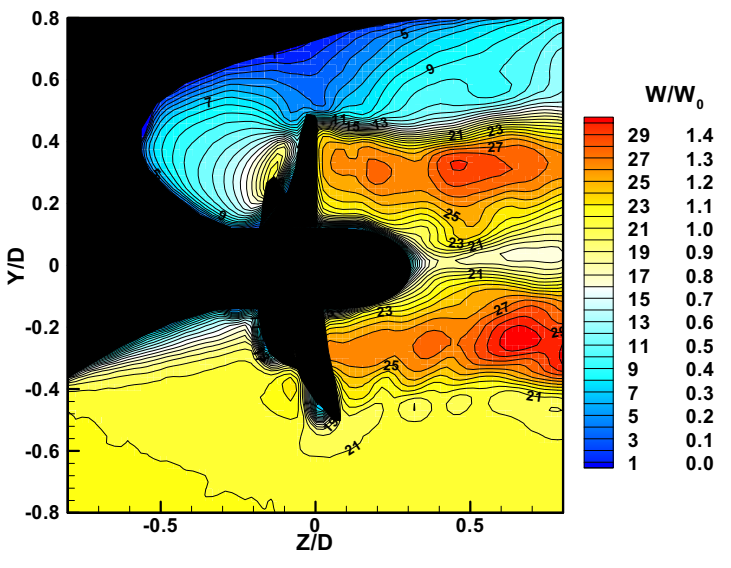

Fig. 5. Contour of phase-averaged axial velocity in the longitudinal plane at ϕ = 0°.

camera. The uncertainty analysis of measurement was carried out for actual particle images for which the velocity field is known in advance. The quiescent flow was tested for the uncertainty evaluation of the present PIV system following the procedure recommended by Raffel et al. (1998). The standard errors encountered in the PIV measurement of displacement vector were calculated and the results are summarized in Table 1. In order to minimize measurement uncertainty, more than 400 instantaneous velocity fields were ensemble averaged in the post-processing routine.

Table 1. Measurement uncertainties of displacement vectors measured by the PIV system.

	Fluctuations (μm)		
	RMS	Min.	Max.
$\sigma_{\Delta z}$	0.061	-6.044	7.468
$\sigma_{\Delta y}$	0.094	-9.384	9.666

The propeller was driven by a servo-motor installed inside the ship model. A 17-bit encoder mounted on the servo-motor generated trigger signals for synchronizing the laser and CCD camera with an accuracy of 0.36° for each selected angular position. Four hundred instantaneous velocity fields were measured at each of four different phases (0°, 18°, 36°, and 54°) using a two-frame PIV method. The reference blade is defined as the phase angle of ϕ = 0° corresponding to the upright position, as shown in Fig. 1(b). The velocity fields for each blade phase were ensemble-averaged to obtain the spatial distributions of the mean velocity, vorticity, and turbulence statistics. Due to space limitations, the results obtained at the phase angle ϕ = 0° were discussed in this paper mainly.

3. Results and Discussion

Figure 4 shows a typical instantaneous velocity field measured in the plane normal to the propeller plane at the phase angle ϕ = 0°. The propeller inflow in the region below the propeller axis (lower inflow region) is nearly uniform. In contrast, the inflow above the propeller axis (upper inflow region) is non-uniform, with a large velocity gradient along the vertical direction. In the upper inflow region, the hull boundary layer is thicker than that in the lower inflow region, which affects the propeller wake and gives rise to various interesting features in the propeller inflow. The axial velocity component in the upper inflow region is very small, whereas the axial velocity in the lower inflow region resembles that of the free stream. In the region behind the propeller, wake sheets are formed

within the slipstream tube, and the wake structure in the upper slipstream (Y/D > 0) shows large variation, compared with that in the lower slipstream.

Figure 5 shows a contour plot of the phase-averaged axial velocity component at the phase angle $\phi = 0°$. The axial velocity distribution differs significantly between the upper and lower inflow regions. In the upper inflow region, the axial velocity increases as the inflow approaches the propeller. In particular, the axial velocity is very low in the region between the propeller blade tip and the hull bottom, a feature that could potentially disturb the smooth passing of the hull wake. In the upper wake region, a strong shear layer is formed at the interface between the propeller slipstream and the hull wake separated from the hull.

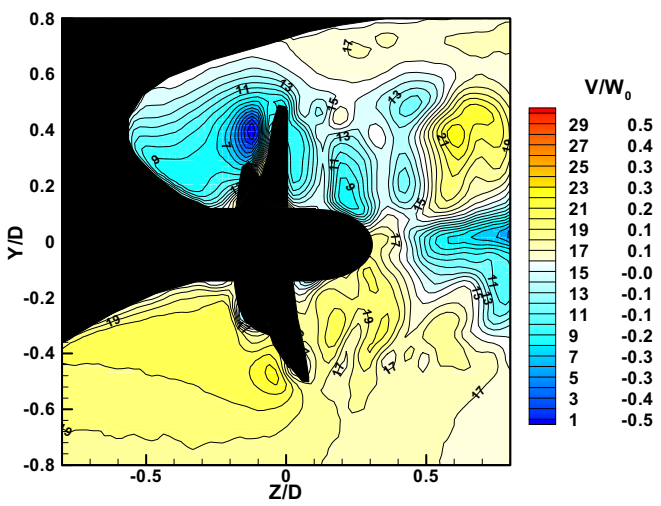

Fig. 6. Contour of phase-averaged vertical velocity at the phase angle $\phi = 0°$.

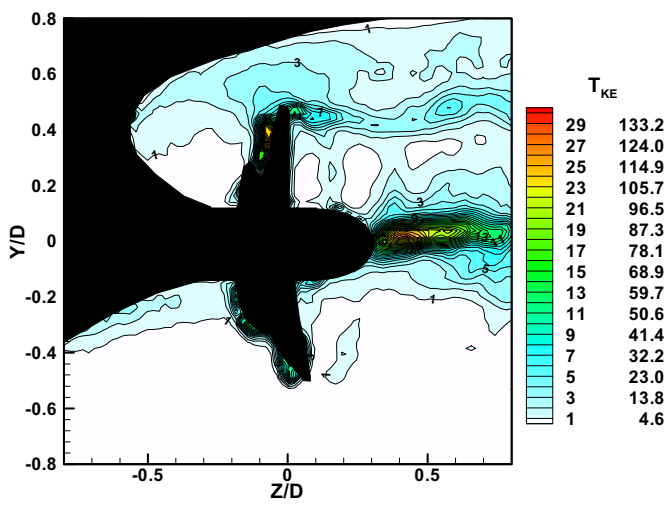

Fig. 7. Contour of phase-averaged turbulence kinetic energy at the phase angle $\phi = 0°$.

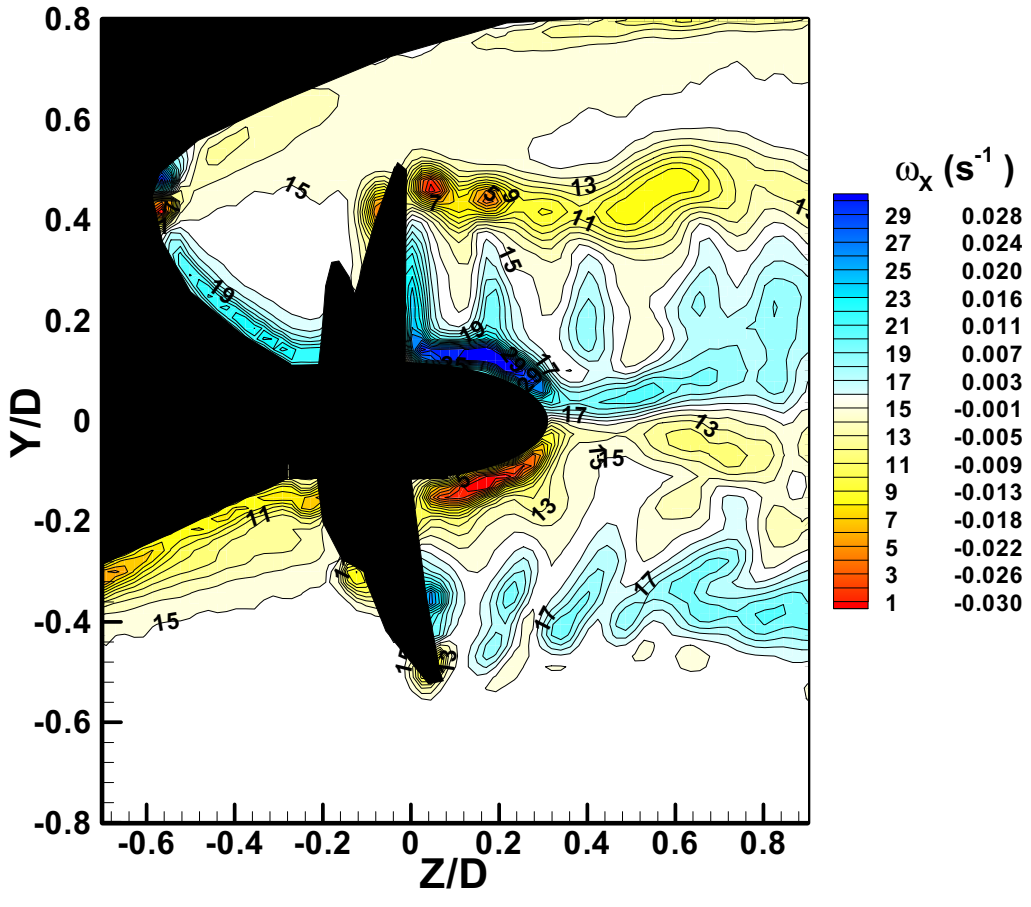

Fig. 8. Contour of phase-averaged vorticity in the longitudinal plane at the phase angle $\phi = 0°$.

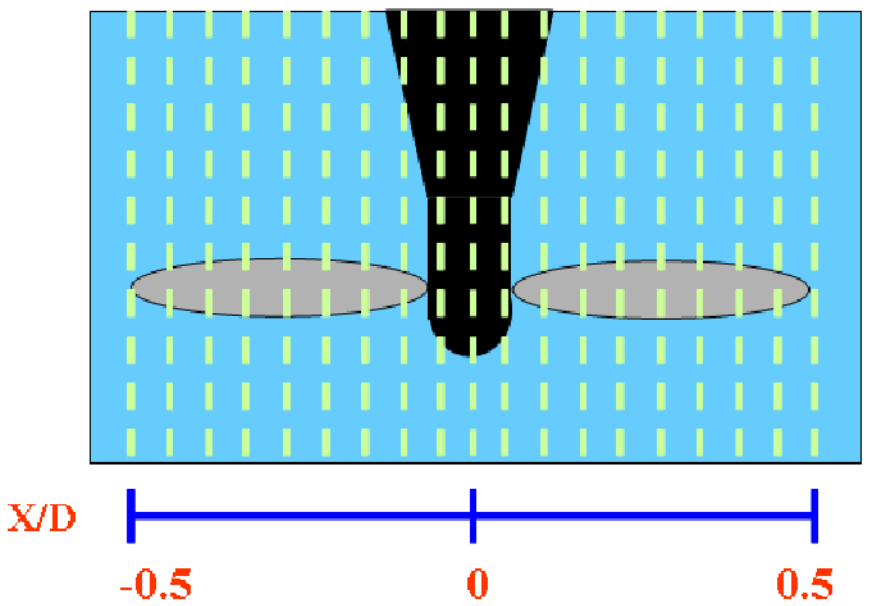

Fig. 9. Measurement planes for total velocity distribution.

Figure 6 shows contour plots of the phase-averaged vertical velocity at $\phi = 0°$. In the upper inflow region, the vertical velocity is negative over a large area, indicating downward motion moving toward the propeller axis, and shows a clear peak at the suction side of the propeller blade. The location of maximum downward flow lies at a height of Y/D = 0.4 and then moves slowly upward as the propeller rotates. The vertical velocity contours in the wake behind the propeller show a pattern similar to that of the inflow region, with negative and positive values dominating in the upper and lower regions, respectively.

The high-speed rotation of the propeller disturbs the inflow and increases the turbulence intensity in the region around the propeller. Assuming that the turbulence structure in the flow around the propeller is isotropic, we calculated the turbulence kinetic energy (T_{KE}) using the in-plane velocity components (W, V). The results are shown in Fig. 7. The T_{KE} has especially large values in the region near the blade tip, trailing and hub vortices. Even though the results at other phase angles were not included due to the space limitation, the T_{KE} in the region between the blade tip and ship hull varies periodically with changing phase angle, which may cause a periodic variation in the pressure on the bottom surface of the ship stern. In the upper region (Y/D > 0), the flow has rather large T_{KE} even behind the propeller plane. In the lower wake region (Y/D < 0, Z/D > 0), however, high viscous dissipation and rapid diffusion cause a substantial decrease of T_{KE}. The difference in the T_{KE} above and below Y/D = 0 can be attributed to large differences in the axial velocity distributions outside the slipstream in the propeller near-wake, as shown in Fig. 5. Additionally, the rotating

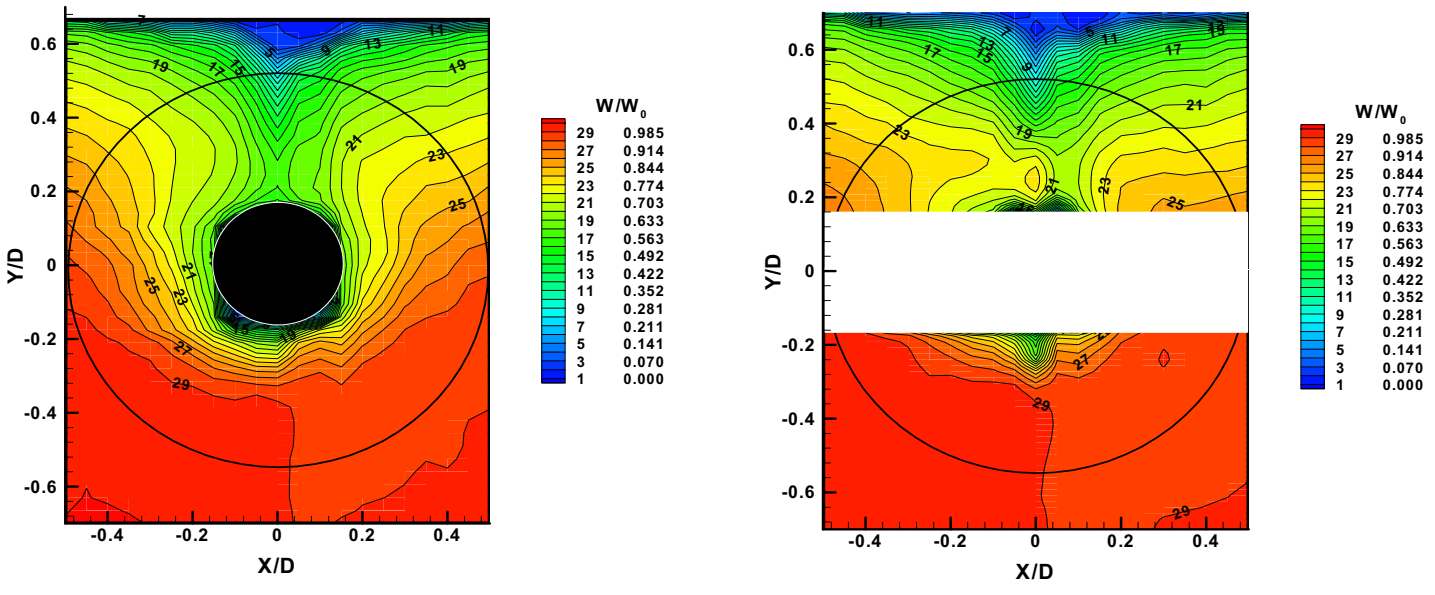

(a) Z/D = –0.3 (b) Z/D = –0.2

Fig. 10. Contour of phase-averaged axial velocity in the transverse planes.

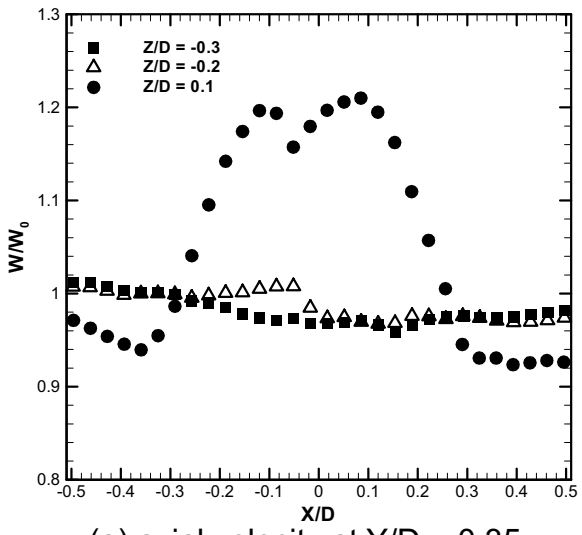

(a) axial velocity at Y/D = 0.35

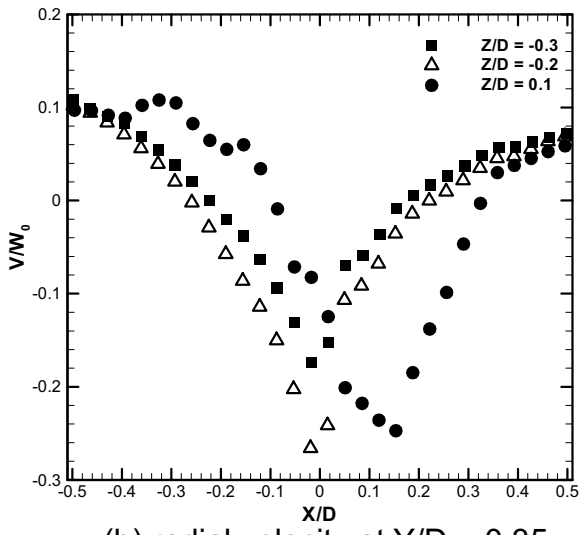

(b) radial velocity at Y/D = 0.35

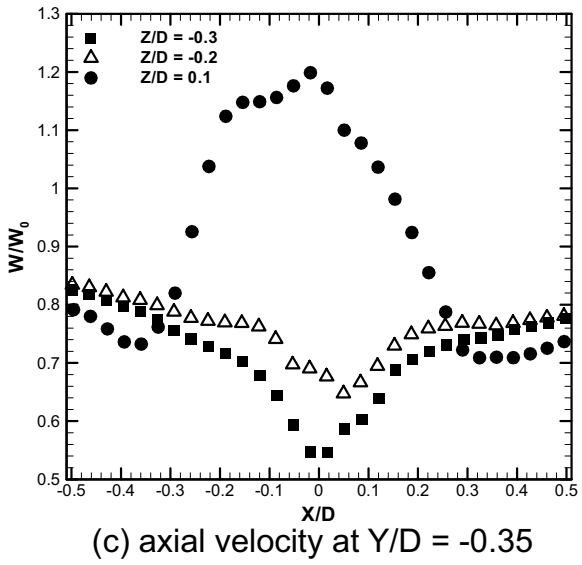

(c) axial velocity at Y/D = -0.35

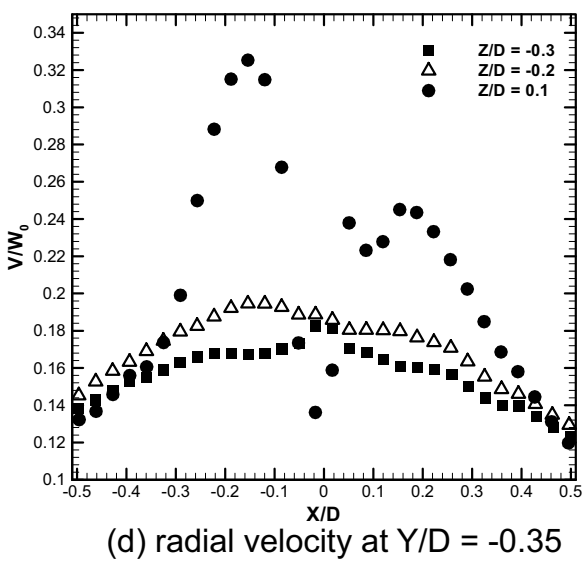

(d) radial velocity at Y/D = -0.35

Fig. 11. Axial and radial velocity profiles in the inflow and wake regions.

propeller causes the T_{KE} distribution of the inflow to be inclined toward the propeller axis in the region of $Y/D < 0$.

Figure 8 shows the phase-averaged vorticity distribution around the propeller at $\phi = 0°$. This plot clearly shows the vortex structure around the rotating propeller. In the inflow region, the vorticity is relatively small except in the area close to the hull. The upper inflow region ($Y/D > 0$) is characterized by nearly negligible vorticity. In the lower inflow region, however, the vorticity has non-negligible values due to the boundary layer developed along the hull bottom surface. In the wake region near the tip, trailing and hub vortices exhibits vorticity values much larger than those in the inflow region. The blade-to-blade interaction between trailing vortices and tip vortices starts at different points in the upper and lower wake regions. The strong upper shear layer between the hull wake and the upper slipstream reduces the convection speed of the tip vortices, causing these vortices to begin interacting with the trailing vortices at about $Z/D = 0.4$. In the lower slipstream, however, the convection speed of the tip vortices is higher than that in the upper slipstream, because the free stream has a higher axial velocity than the hull wake above the upper slipstream; these effects cause the interaction between the tip and trailing vortices to be triggered at about $Z/D = 0.5$. As the flow passes the downstream location of $Z/D = 0.2$, the vorticity value of the tip vortices decreases rapidly in the lower slipstream. From this, we can see that the vortex structure dissipates faster in the lower slipstream than in the upper slipstream due to the large magnitude of the free stream velocity.

The total velocity distributions were measured at 21 longitudinal planes covering the range of $-0.5 < X/D < 0.5$. Figure 9 shows the measurement planes for the extraction of total velocity distribution. The lateral spacing between adjacent measurement planes was 2.7 mm. First, the axial velocity distribution for each longitudinal plane at $\phi = 0°$ was measured. Then, the axial velocity profiles for all 21 longitudinal planes were combined at the transverse planes of $Z/D = -0.2$ and -0.3,

as shown in Fig. 10. The contour plot of the phase-averaged axial velocity at the transverse cross-section of Z/D = -0.3 shows a slightly asymmetric distribution, with larger axial velocities on the port side. For wake behind a bare hull, the hull wake exhibits a symmetric velocity distribution; however, when the propeller is operating, the total velocity has an asymmetric distribution, even if the upstream location is far from the propeller plane, as shown in Fig. 10(a). This asymmetry in the axial velocity distribution is enhanced as the inflow approaches the propeller plane. At Z/D = -0.2, we had difficulty in extracting velocity vectors in the area around the propeller boss ($-0.16 < Y/D < 0.16$) due to severe reflection and scattering of laser light from the hull surface. The propeller rotation causes the axial velocity of the inflow on the port side ($X/D < 0$) to be greater than that on the starboard side ($X/D > 0$). In addition, this leads to a greater total area with axial velocity greater than $0.8W_0$ on the port side compared to the starboard side. The inflow onto the propeller blade is non-uniform, especially around the upright position ($X/D = 0$). The asymmetric and non-uniform feature of the inflow ahead of the rotating propeller may cause the loading on each propeller blade to be different.

To investigate the inflow structure in detail, axial and radial velocity profiles were extracted at $Y/D = \pm 0.35$, which is the very important position because propeller designers usually locate the maximum loading of propeller blade at Y/R = 0.7. Figures 11(a) and (b) show the characteristics of inflow very well. Although the inflow had symmetric axial velocity profile at the far inflow region of Z/D = -0.3, it deformed soon at Z/D = -0.2 because it felt the operation of propeller. The axial velocity profile of inflow informed of the thick hull wake. Especially, as the bilge vortex of port side encountered the rotating propeller in the same direction of it, axial velocity of port side increased more than that of starboard side and the center of inflow was shifted to the starboard side. The region of slipstream was $-0.35 \le X/D \le 0.35$. The inflow showed the continuous velocity profile at the boundary of slipstream, however, the wake showed discontinuous velocity profile because of the generation of tip vortices and the difference of axial momentum between slipstream and free stream regions. The radial velocity profile also showed the effects of the rotating propeller. The inflow at Z/D = -0.2 had strong negative radial velocity and kept rather symmetric shape. From this, it can be said that the propeller operation deformed the axial inflow velocity profile more than the vertical inflow velocity profile and opposite situation occurred in the wake region. The axial velocity profiles of the lower inflow region were neither affected seriously by the hull wake nor propeller rotation as shown in Fig. 11(c). The magnitude of axial velocity was similar to that of free stream and small radial velocity occurred at Z/D = -0.2 and -0.3. The significant difference of velocity profiles between upper and lower regions may happen to make a face cavitation at lower blade region because of the very small angle of attack and large relative inflow velocity to the blade. As the face cavitation can result in the erosion on blade surface, the decrease of propulsion and the vibration of blade itself, it has been considered as the dangerous state in propulsion performance. Recently, the vessels such as chemical tanker or LNG carrier which have fat stern, however, they require higher propulsion such that they have much possibility of face cavitation. The detailed investigation of propeller inflow, based on the numerical simulation and the flow visualization, would be helpful for the design of the safe and fast vessel.

Previous experimental results measured by LDV or Pitot tubes do not contain spatially resolved velocity field information because of the complicated geometry of a ship stern and a propeller. They also do not provide detailed flow structure of propeller inflow such as the presence of vortices near hull bottom, asymmetric evolution of inflow, non-uniform inflow distribution and interaction between blade and ship hull. This experimental result would be very helpful to verify the current numerical codes, although those were obtained at low Reynolds number.

4. Conclusion

The flow characteristics around a rotating propeller attached to a KRISO 3600TEU container ship model were visualized and investigated using a PIV technique. Phase-averaged mean velocity fields in the longitudinal planes were obtained at four different blade phases.

The hull wake of low axial velocity above the propeller axis affects the inflow structure, accelerating the inflow and generating strong wake sheets in the upper slipstream. The vorticity is relatively small in the inflow ahead of the propeller, except for the boundary layer near the hull. However, the vorticity is large in the regions containing the tip, trailing and hub vortices in the

near-wake behind the propeller. The inflow showed the continuous velocity profile at the boundary of slipstream. The total velocity distribution of the inflow is non-uniform and asymmetric with respect to the propeller boss. The inflow just behind of the propeller plane had strong negative radial velocity. The longitudinal bilge vortex of port side increased the axial velocity more than starboard side and the center of inflow was shifted to the starboard side. This asymmetric inflow structure could potentially act as a major source of cavitation, noise, and pressure fluctuations on the hull. Therefore, detailed information on the inflow structure, especially the total velocity distribution, would be useful for optimizing propeller design.

Acknowledgment

This work was supported by National Research Laboratory Program of Ministry of Science and Technology (MOST) and was sponsored by the Ministry of Commerce, Industry and Energy (MOCIE), Korea under the project code PN00770.

References

Kuiper, G., Grimm, M., Mcneice, B., Noble, D. and Krikke, M., Propeller inflow at full scale during a manoeuvre, Proceedings: 24th Symposium on Naval Hydrodynamics (Fukuoka), 2 (2002) 234-249.

Lauden, J., The influence of the propeller on the wake distribution as established in a model test, the Society of Naval Architects and Marine Engineers, Propeller `81 Symposium (Vergina), (1981), 233-242.

Lee, C. S., Kim, Y. G. and Ahn, J. W., Interaction between a propeller and the stern shear flow, Korea-Japan Joint Workshop on Hydrodynamics in Ship Design, (1991), 16-29.

Lee, S. J., Paik, B. G. and Lee, C. M., Phase-averaged PTV measurements of propeller wake, JOURNAL OF SHIP RESEARCH, 49-1, (2004a), 43-54.

Lee, S. J., Paik, B. G., Yoon, J. H. and Lee, C. M., Three component velocity field measurements of propeller wake using stereoscopic PIV technique, Experiments in fluids, 36-4, (2004b), 575-585.

Paik, B. G., Lee, C. M. and Lee, S. J., PIV analysis of flow around a container ship model with a rotating propeller, Experiments in Fluids, 36-6, (2004), 833-846.

Raffel, M., Willert, C. and Kompenhans, J., Particle Image Velocimetry, (1998), Springer, ISBN 3-540-63683-8.

Author Profile

Bu Geun Paik: He received his master degree in Physics in 1995 from POSTECH and worked as a research engineer in Samsung Shipbuilding Company. He received Ph.D. in Mechanical Engineering in 2005 from the same university. He has worked in Marine Transportation Safety Research Division of MOERI(KORDI) as a senior research scientist since 2004. His research interests are ship hydrodynamics and turbulence control using active or passive methods.

Gun Do Kim: He received his master and Ph.D. in Naval Architecture and Ocean Engineering from Chungnam National University in 1999 and 2003, respectively. He has worked in Marine Transportation Safety Research Division of MOERI(KORDI) as a senior research scientist since 2005. His research interests are ship hydrodynamics and propeller cavitation control and analysis.

Jung Yeop Lee : He received his master degree in Mechanical Engineering in 2005 from POSTECH. He is a Ph. D student at POSTECH and his research interests are turbulent flow control using active methods and micro- or bio-fluid.

Sang Joon Lee: He received his master and Ph.D. in Mechanical Engineering from KAIST (Korea Advanced Institute of Science and Technology) in 1982 and 1986, respectively. In 1986 he worked as a senior researcher at KIMM. He is currently a professor in the Department of Mechanical Engineering at POSTECH after joining as an assistant professor in 1987. His research interests are quantitative flow visualization (PIV, PTV, LIF, Holography), experimental fluid mechanics, bluff body aerodynamics, microfluidics and flow control